aerospace

MDPI

Article

Synthesis and Experimental Characterization of a MWCNT-Filled Bio-Based Adhesive

Konstantinos Tserpes *,† and Vasileios Tzatzadakis *,†

Laboratory of Technology & Strength of Materials, Department of Mechanical Engineering & Aeronautics, University of Patras, 26500 Patras, Greece

* Correspondence: kitserpes@upatras.gr (K.T.); vasileios.tzatzadakis@upnet.gr (V.T.)

† These authors contributed equally to this work.

Abstract: In the present paper, a novel epichlorohydrin/cardanol adhesive was reinforced by multi-walled carbon nanotubes (MWCNTs) and characterized experimentally. The adhesive was reinforced by MWCNTs in weight ratios (wt %) of 0.5%, 1.0% and 2.0%. The bulk properties of the reinforced adhesive were characterized through dynamic mechanical analysis tests, tension tests, and fracture toughness tests, while its shear behavior was characterized through single-lap shear tests on aluminum and composite bonded specimens. The morphology of the reinforced adhesive was characterized using scanning electron microscopy tests. Due to the high viscosity of the bio-based adhesive, special efforts were placed on the dispersion of the MWCNTs into the adhesive, which was achieved through mechanical mixing. The results from the tests show that the presence of the MWCNTs increases the glass transition temperature, the Young's modulus and the fracture toughness of the reinforced bio-based adhesive, while it decreases its tensile strength. This contradictory finding is attributed to the formation of MWCNT agglomerates into the adhesive. For the content of 2.0 wt %, the shear strength of the reinforced adhesive is increased by 57% for the aluminum joints and by 10.4% for the composite joints. The findings of the study reveal that the reinforcement of the bio-based adhesive by MWCNTs is feasible from a manufacturing viewpoint and may increase the efficiency of the adhesive in structural applications.

Keywords: bio-based adhesive; epichlorohydrin; cardanol; multi-walled carbon nanotubes; mechanical testing; bonded joints

Citation: Tserpes, K.; Tzatzadakis, V. Synthesis and Experimental Characterization of a MWCNT-Filled Bio-Based Adhesive. *Aerospace* **2021**, *8*, 26. https://doi.org/10.3390/aerospace8020026

Academic Editor: Konstantinos Kontis

Received: 23 December 2020

Accepted: 19 January 2021

Published: 21 January 2021

1. Introduction

In the last decades, the epoxy-adhesive applications are expanding very fast to interior (cosmetic) and secondary structural applications in the aerospace [1,2], the automotive industries [3] and used in the construction industry in a semi-cured state [4]. At the same time, the new environmental restrictions are asking for polymers of lower environmental footprint, decreased production cost and increased recyclability [4,5]. The environmentally friendly polymers are divided into the bio-based polymers and the bio-degradable polymers [6]. The bio-based polymers are derived from natural renewable resources, such as plants and fruits. One of the main drawbacks of bio-based polymers are their low mechanical properties. A method to enhance the mechanical properties of bio-based polymers is to reinforce them by nanoparticles. In this direction, many works have been reported in the literature for conventional epoxy resins and adhesives, e.g., [7–9]. On the other hand, the bio-degradable polymers cannot be used as structural epoxy resins or adhesives due to the degradation of their physical properties when exposed to a humid environment and UV radiation [10,11].

In [12], the authors have produced and characterized a novel bio-based adhesive made from epichlorohydrin and cardanol. The main source of epichlorohydrin is glycerin. Since glycerin is plant-based, the production of epichlorohydrin from glycerin (or glycerol) is cost-efficient and also environmentally friendly [13]. The glycerin to epichlorohydrin

process is more energy-efficient, due to simpler chemical procedures, and there are no hazardous wastes to deal with [13]. Cardanol is a chemical compound produced from anacardic acid, which is found in the cashew nutshell liquid. The mechanical characterization has shown that the properties of the epichlorohydrin/cardanol adhesive fulfill the property requirements of structural adhesives [14] and are very close to the average property values of commercial structural adhesives.

Given that the bio-based polymers are prone to environmental conditions, in [15], the effects of hygrothermal ageing on the mechanical properties of the epichlorohydrin/cardanol adhesive have been characterized experimentally by subjecting bulk specimens and bonded joints to the conditions of 70 °C/RH85% until saturation and then testing them mechanically. It was found that the epichlorohydrin/cardanol adhesive is prone to hygrothermal ageing since its bulk properties are considerably decreased. However, this is not the case for the shear strength measured from single-lap shear tests on aged bonded specimens.

In the present work, the epichlorohydrin/cardanol adhesive was filled by multi-walled carbon nanotubes (MWCNTs) aiming to enhance its mechanical properties, thus making it more suitable for structural applications. Three different MWCNT contents, namely 0.5, 1.0 and 2.0 wt % were applied. The reinforcement efficiency was tested by means of dynamical mechanical analysis (DMA) tests, tension tests, fracture toughness tests on bulk specimens and single-lap shear (SLS) tests on bonded specimens. The morphology of the MWCNT-filled adhesive was characterized by scanning electron microscopy (SEM) tests.

2. Materials

The bio-based adhesive was obtained by a synthesis of three compounds: the EnviPOXY-530 epoxy resin (SPOLCHEMIE, Labem-město, Czech Republic), the NX-2003 curing agent (CARDOLITE CO., Gent, Belgium), and the NC-513 reactive diluent (CARDOLITE CO., Gent, Belgium). The epoxy resin is made from epichlorohydrin, which is based on glycerol. The hardener is a phenalkamine curing agent with no benzyl alcohol compounds, which provides excellent adhesive properties to the resin matrix due to the cashew liquid chemical structure. The reactive diluent is derived from natural and renewable feedstock and is based on cardanol. It provides the resin system with flexibility and it is solvent-free. For the single-lap bonded joints, two types of adherents were selected: metallic adherents made from aluminum 2024-T3 and composite adherents made from the UD prepreg M21/T800 material. The thickness of the aluminum adherents is 1.15 mm. The lay-up of the composite adherents is [(0/45/90/−45)3]s and their thickness is 2.5 mm. The MWCNTs used were the COOH Functionalized Multi Walled Carbon Nanotubes (Cheap Tubes Inc., Grafton, MA, USA). They have an external diameter range of 10–20 nm, an internal diameter range of 3–5 nm, and a purity of more than 95%.

3. Experimental

3.1. Synthesis of the MWCNT-Filled Adhesive and Production of Bulk Samples

The epoxy resin was mixed with the reactive diluent and the MWCNTs, and the mixture was pre-heated at 55 °C into a glass borosilicate beaker. Then, the mixture was stirred mechanically using a Dispermat Dissolver VL1 (VMA-Getzmann, Brüchermühle, Germany) for 20 min at 2000 rpm in a vacuum to homogenize the mixture and disperse the MWCNTs into the resin. Similarly, the hardener was heated to 55 °C and was degassed in a vacuum. The epoxy mixture was placed into an ultrasonic bath (Elmasonic P, Elma Schmidbauer GmbH, Singen, Germany) at 65 °C for 20 min in order to improve the MWCNTs dispersion. Then, an additional degassing was performed from the epoxy mixture and the hardener using ultrasonics. After the recovery of the epoxy mixture and the hardener to the room temperature, the two components were mechanically mixed inside the ultrasonic bath for 10–15 min. The synthesis process of the MWCNT-filled adhesive is illustrated in Figure 1.

Figure 1. Photographic illustration of the synthesis process of the multi-walled carbon nanotube (MWCNT)-filled adhesive.

To produce the bulk adhesive specimens, two silicone molds were manufactured according to the ASTM standards from high-temperature tolerant silicone. The MWCNT-filled adhesive was poured into the molds' cavities while the molds were pre-heated at 55 °C. The curing cycle applied to the adhesive was 6 h at 80 °C and the post-curing was 8 h at 140 °C.

3.2. Surface Treatment and Production of Bonded Specimens

The surface of the aluminum adherents was treated both mechanically using sandpaper and chemically. For the sanding process, a 400-grit sandpaper was used. After the sanding, the adherents were washed-off into a bath of deionized water and brushed with gauze fabric followed by a 10 min ultrasonic cleaning bath at 37 kHz. The chemical treatment was applied according to the ASTM D3933 standard. The adherents were brushed with acetone (solvent clean), and afterwards, immersed into a sodium hydroxide solution (NaOH 5 wt %) for 10 min at 25 °C (alkaline clean). Subsequently, they were immersed into a deionized water bath for 10 min at 60 °C. Nitric acid solution (HNO_3 32.5 wt %) was used as a deoxidizer. The adherents were immersed into the nitric acid solution for 8 min at 25 °C. Subsequently, they were immersed into a deionized water bath for 10 min at 25 °C. The anodizing process was carried out into a phosphoric acid solution (H_3PO_4 12 wt %). For each adherent, one stainless steel rod, which has been thoroughly cleaned by acetone, was immersed inside the phosphoric solution alongside the adherent. Afterwards, the anodizing procedure has taken place for 23 min at room temperature. Finally, the aluminum adherents were immersed into deionized water for 10 min and dried inside a contamination-free oven for 1 h at 40 °C.

The surface of the composite adherents was treated manually with sandpaper. The sanding process took place while the specimens were immersed into deionized water. In this way, the dust residuals of the composites were washed away by the water, thus optimizing the sanding outcome. 220-grit and 320-grit sandpapers were used. After the sanding process, the coupons were washed off with deionized water. A soft brushing was followed using a wet thin gauze fabric. Finally, the composite adherents were dried for 8 h at 60 °C inside an oven, and the bonding surface was cleaned carefully with acetone.

The bio-based adhesive was applied carefully to the adherents. The bonding area is 30 × 25.4 mm and 25.4 × 25.4 mm for the composite and aluminum joints, respectively. The adherents were bonded together and cured for 6 h at 80 °C, followed by a post-curing process of 8 h at 140 °C while a mechanical pressure was applied to the bonded area.

3.3. Characterization

3.3.1. DMA Tests

A DMA Q800 V7.0 instrument with a 3-point bending clamp was used to conduct the DMA tests on the aged epichlorohydrin/cardanol adhesives for evaluating its ther-

momechanical properties. A thermal cycle from 25 °C up to 140 °C, with a heating rate of 10 °C/min under air, was applied. A sample of dimensions of 50 × 4.4 × 3.1 mm was used. The DMA specimen was shaped from a tension coupon, which is used for the tension test. The tension coupon is machined to the desired dimensions. The DMA coupon, in comparison to the dog-bone tension specimen, is shown in Figure 1. The test apparatus and the mounted DMA coupon are illustrated in Figure 2. The test was performed using sinusoidal strain and frequency of 1 Hz.

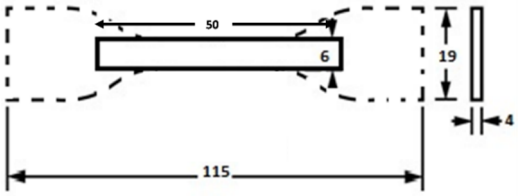

Figure 2. Sketch and dimensions (in mm) of the dynamical mechanical analysis (DMA) and dog-bone tension samples.

3.3.2. Tension Tests

The tension tests were conducted according to the ASTM D638-14 standard using a Tinius Olsen tensile tester with a load cell of 5 kN. The type-IV dog-bone samples were used. The sketch and dimensions of the dog-bone tension sample are also shown in Figure 2 with the dashed line. The tests were conducted at a loading rate of 1 mm/min. Five specimens were tested in total.

3.3.3. Fracture Toughness Tests

For the characterization of the Mode-I fracture toughness of the aged epichlorohydrin/cardanol adhesive, single edge notched bend (SENB) samples were used. The geometry and dimensions of the SENB samples are shown in Figure 3. The width of the specimens was 3 mm. The tests were conducted according to the ASTM D5045-14 standard using a Tinius Olsen machine. Prior to the tests, a 3 mm pre-crack (notch) has been created on the specimens using a razor-sharp blade placed on the machine's grip and applying a relatively slow load rate (0.1 mm/min). In total, three specimens were tested using a 1.0 mm/min loading rate.

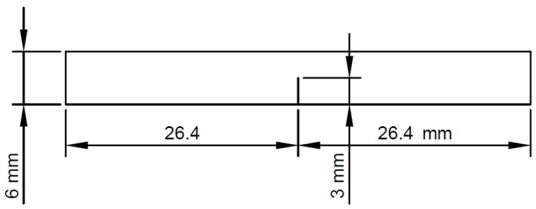

Figure 3. Sketch and dimensions (in mm) of the SENB sample.

Mode-I fracture toughness was evaluated in terms of the critical stress intensity factor K_{IC} and the critical energy release rate G_{IC} [16]. K_{IC} is derived at the tip of the notch at the fracture initiation load by

$$K_{IC} = \left(\frac{P_Q}{BW^{\frac{1}{2}}}\right) f(x) \quad (1)$$

where P_Q is the load (kN), B is the specimen's thickness (cm), W is the specimen's depth (cm), $x = a/w$, a is the crack length (cm),

$$f(x) = 6x^{1/2} \frac{[1.99 - x(1-x)(2.15 - 3.93x + 2.7x^2]}{(1+2x)(1-x)^{3/2}} \quad (2)$$

while G_{IC} is derived from:

$$G_{IC} = \frac{(1-\nu)K_{IC}^2}{E} \quad (3)$$

where ν is the Poisson's ratio, K_{IC} is the stress intensity factor and E is the Young's modulus.

3.3.4. SLS Tests

The bonding capability of the nano-reinforced epichlorohydrin/cardanol adhesive was evaluated by means of the lap shear strength (LSS) which was measured by lap-shear tests conducted on composite and aluminum bonded joints, according to ASTM D5868-01 and ASTM D1002-10 standards, respectively. The LSS tests were conducted using an MTS 100 kN testing machine at a loading rate of 1 mm/min. Five specimens were tested for each case. The dimensions of the carbon fibre reinforced polymer (CFRP) adherents are 100 × 25.4 × 2.5 mm (Figure 4a) and the dimensions of the aluminum adherents are 101.6 × 25.4 × 2.5 mm (Figure 4b). The overlap length was 25 mm for the CFRP specimens and 25.4 mm for the aluminum specimens. In both cases, 25.4 × 25.4 mm tabs were used.

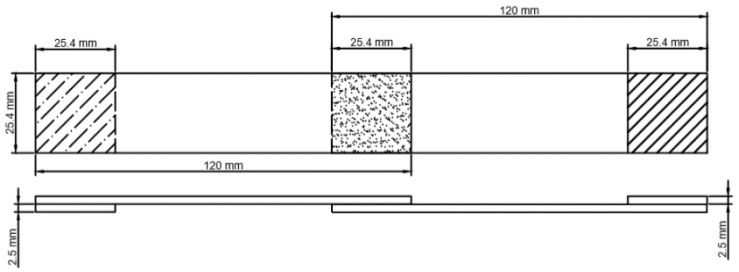

(**a**)

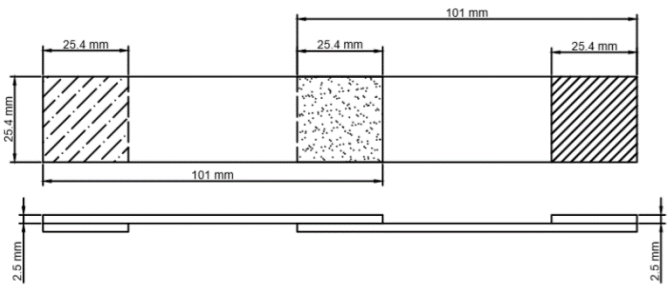

(**b**)

Figure 4. Sketches and dimensions (in mm) of the aluminum SLS specimen (**a**) and the CFRP single-lap shear (SLS) specimen (**b**).

4. Experimental Results

4.1. SEM Observation

Before conducting the mechanical tests, the morphology of the MWCNT-filled adhesive was investigated using SEM analysis. Figure 5 depicts representative SEM images for the three MWCNT-filled adhesives. The examination of the SEM images has revealed the presence of MWCNT agglomerations despite the special effort spent in the production process to optimize the MWCNTs dispersion. This is mainly due to the high viscosity of the bio-adhesive compared to other polymer matrices. As indicated in Figure 5 by the red the arrows, with increasing the MWCNT content the size and population of the agglomerations increase as well.

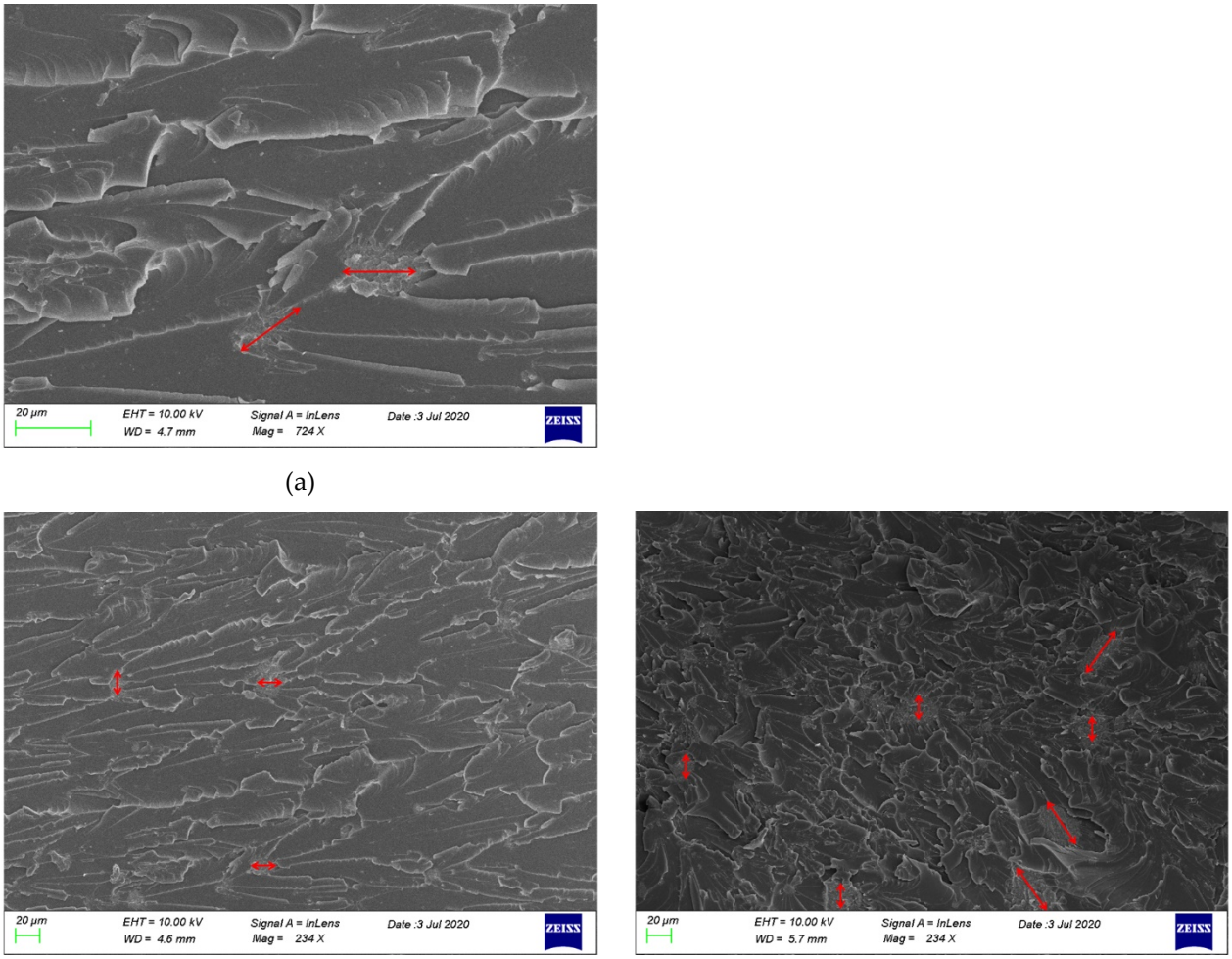

Figure 5. SEM images of the MWCNT-filled adhesive: (**a**) 0.5 wt %, (**b**) 1.0 wt % and (**c**) 2.0 wt %.

4.2. Glass Transition Temperature

Figure 6 compares the T_g values of the MWCNT-filled adhesives with the value of the neat adhesive. As shown, the addition of MWCNTs leads to a small but considerable increase of the T_g by 1.3%, 3.6% and 5.6% for the reinforcements of 0.5 wt %, 1.0 wt % and 2.0 wt %, respectively. The experimental results are shown in Figure 7. The increase is due to the partial immobilization of the polymeric rings by the MWCNTs and the formation of hydrogen bonds between the adhesive and the MWCNTs [17].

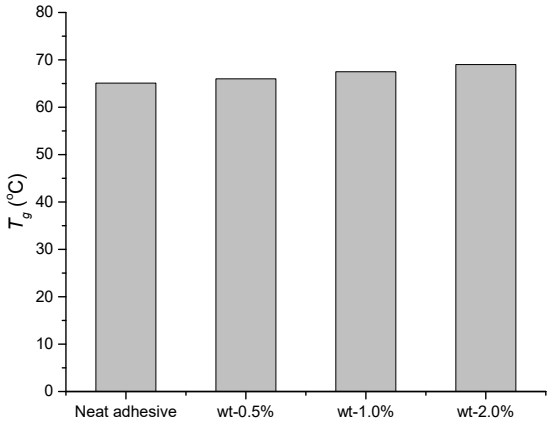

Figure 6. Comparison of the T_g of the MWCNT-filled adhesives and the neat adhesive [12].

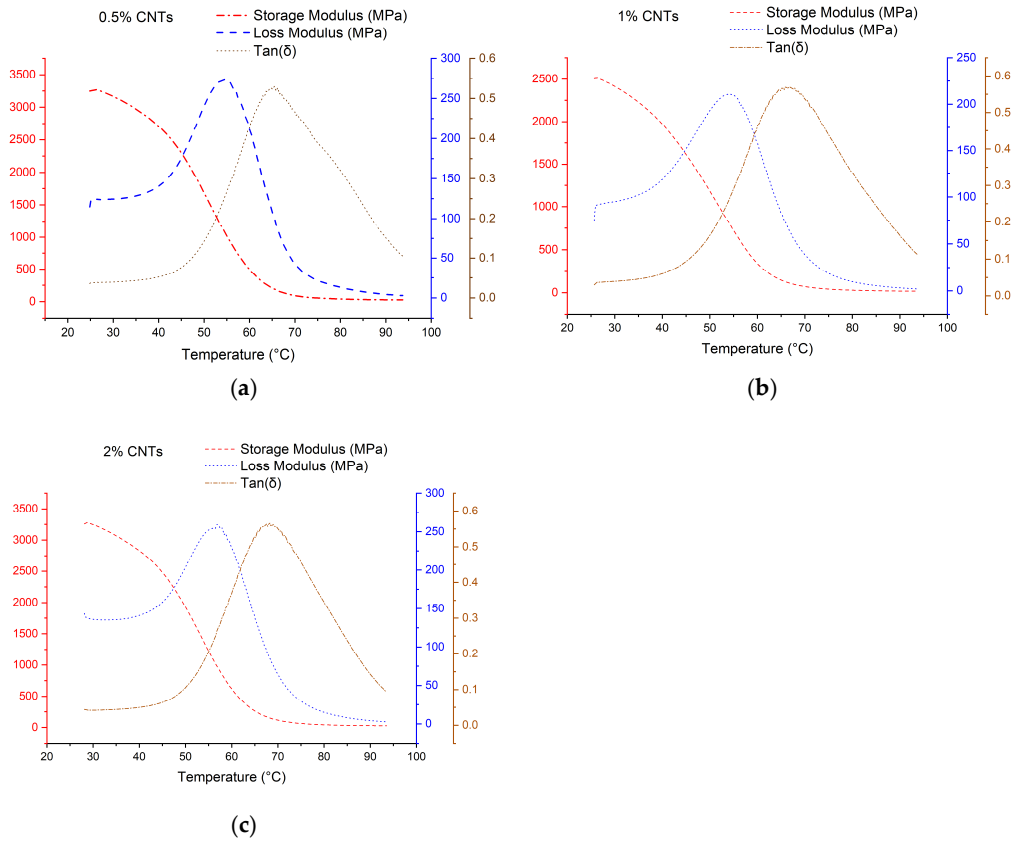

Figure 7. DMA results of the MWCNT-filled adhesive: (**a**) 0.5 wt %, (**b**) 1.0 wt % and (**c**) 2.0 wt %.

4.3. Tensile Behavior

Figure 8 displays the stress–strain curves from the tension tests on the MWCNT-filled adhesive samples. The MWCNT-filled adhesive shows an elastoplastic behavior. The Young's modulus was determined by slopes, which were calculated on the initial linear portion of the curve using least-squares fit on test data (5 to 25 MPa). The deviation between the curves is acceptable.

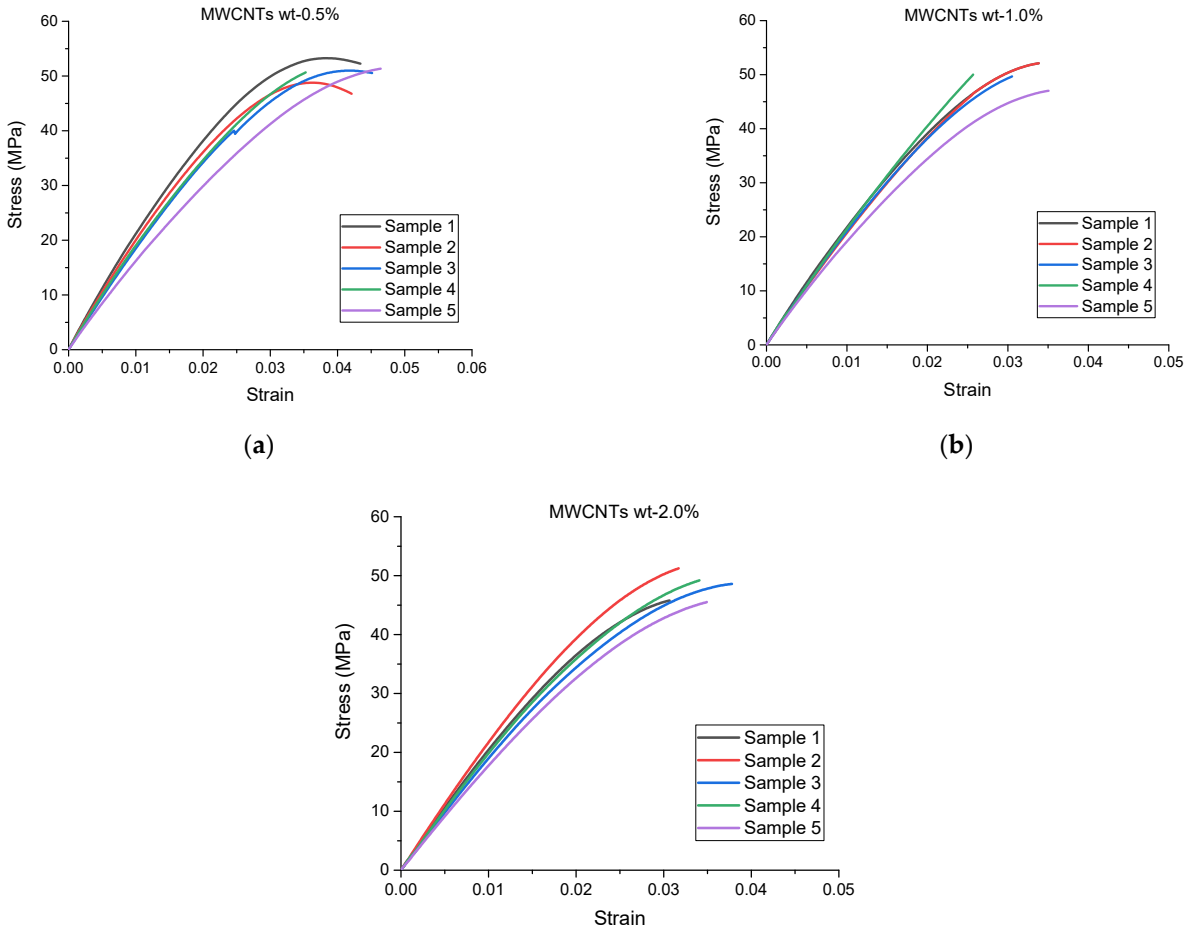

Figure 8. Tensile stress–strain curves of the MWCNT-filled adhesive: (**a**) MWCNTs 0.5 wt %, (**b**) MWCNTs 1.0 wt %, (**c**) MWCNTs 2.0 wt %.

Figure 9 compares the average Young's modulus of the MWCNT-filled adhesives with that of the neat adhesive [12]. The Young's modulus was extracted from the initial part of the curves using the least-squares linear regression method. The comparison shows that the addition of the MWCNTs causes an increase of the Young's modulus of the MWCNT-filled adhesive by 2.7%, 5.3% and 6.4% for the reinforcements of 0.5, 1.0 and 2.0 wt %, respectively. The increase is due to the high Young's modulus of the MWCNTs. Also, the addition of the MWCNTs increases the standard deviation values of Young's modulus, which is due to the variation of material's formulation and the formation of the agglomerates. Table 1 displays the time to failure for the tension tests.

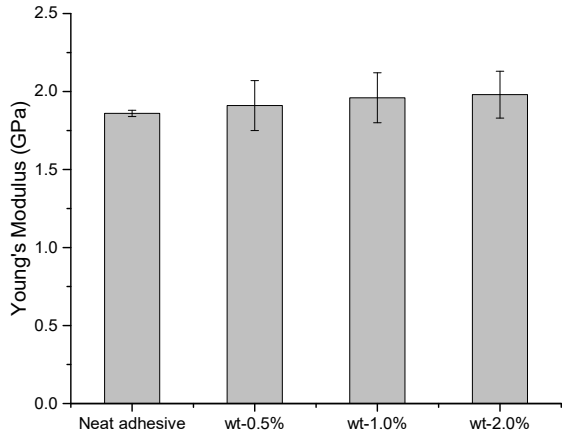

Figure 9. Comparison of the Young's modulus of the MWCNT-filled adhesive and the neat adhesive [12].

Table 1. Time to failure for the tension tests.

0.5% CNTs		1% CNTs		2% CNTs	
Sample 1	2.82 min	Sample 1	2.19 min	Sample 1	1.99 min
Sample 2	2.73 min	Sample 2	2.14 min	Sample 2	2.06 min
Sample 3	2.80 min	Sample 3	1.95 min	Sample 3	2.45 min
Sample 4	2.27 min	Sample 4	1.65 min	Sample 4	2.21 min
Sample 5	3.01 min	Sample 5	2.27 min	Sample 5	2.27 min

Figure 10 compares the average tensile strength of the MWCNT-filled adhesives with that of the neat adhesive [12]. The tensile strength was taken equal to the maximum stress in the curves. The comparison shows that the addition of the MWCNTs causes a decrease of the tensile strength of the MWCNT-filled adhesive by 15%, 19% and 20.6% for the reinforcements of 0.5, 1.0 and 2.0 wt %, respectively. The decrease is due to the presence of agglomerations which act as defects in the material. Similar findings regarding the negative effect of the MWCNT agglomerations have been also reported in [18,19].

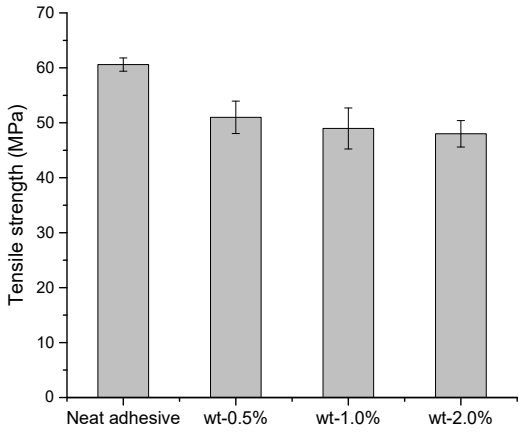

Figure 10. Comparison of the tensile strength of the MWCNT-filled adhesive and the neat adhesive [12].

Figure 11 illustrates a failed tension specimen made from the MWCNT-filled adhesive. This is a representative failure mode for all tension specimens.

Figure 11. Fractured tension specimen.

4.4. Fracture Toughness

Figure 12 displays the force-displacement curves obtained from the fracture toughness tests conducted on the MWCNT-filled adhesive SENB samples. Between the curves, an acceptable deviation is achieved. Figure 13 compares the average values of the K_{IC} of the MWCNT-filled adhesives with that of the neat adhesive [12]. The comparison shows that the addition of the MWCNTs causes an increase of the K_{IC} by 1.3%, 3.9% and 7.2% for the reinforcements of 0.5, 1.0 and 2.0 wt %, respectively. The increase is due to the crack bridging and crack turning caused by the presence of the MWCNTs. In Figure 14 is shown a representative a case where the main crack was enforced to split into two cracks by the MWCNTs which were located in front of the crack tip.

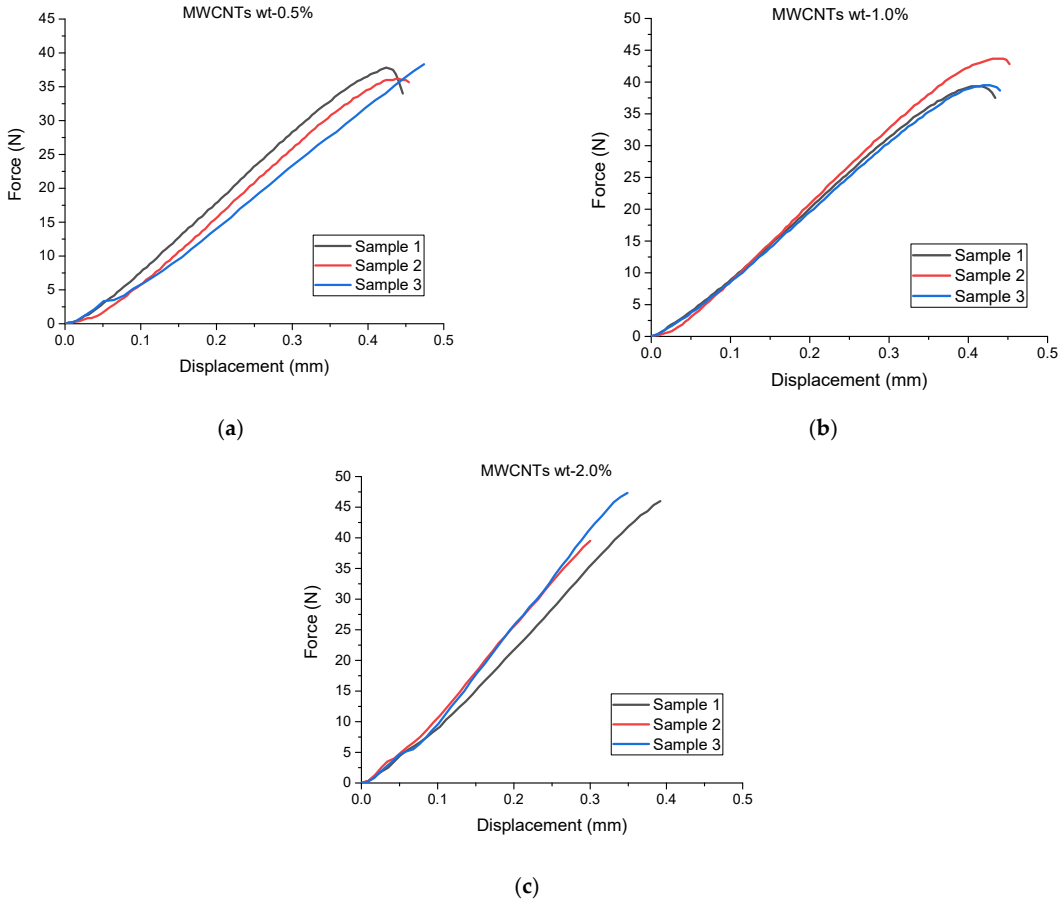

Figure 12. Force-displacement curves of the MWCNT-filled single edged notched bend (SENB) samples: (**a**) 0.5 wt %, (**b**) 1.0 wt %, (**c**) 2.0 wt %.

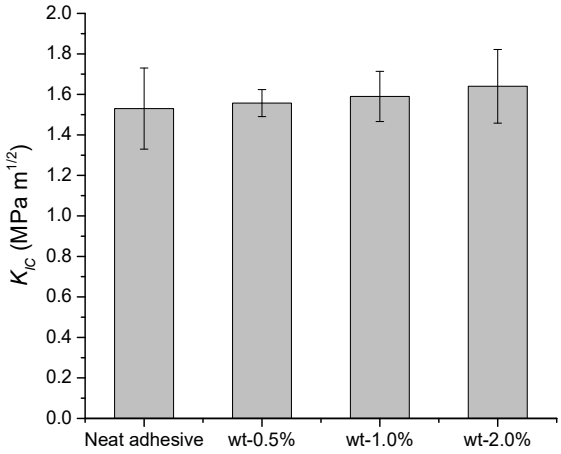

Figure 13. Comparison of the K_{IC} of the MWCNT-filled SENB samples with that of the neat adhesive [12].

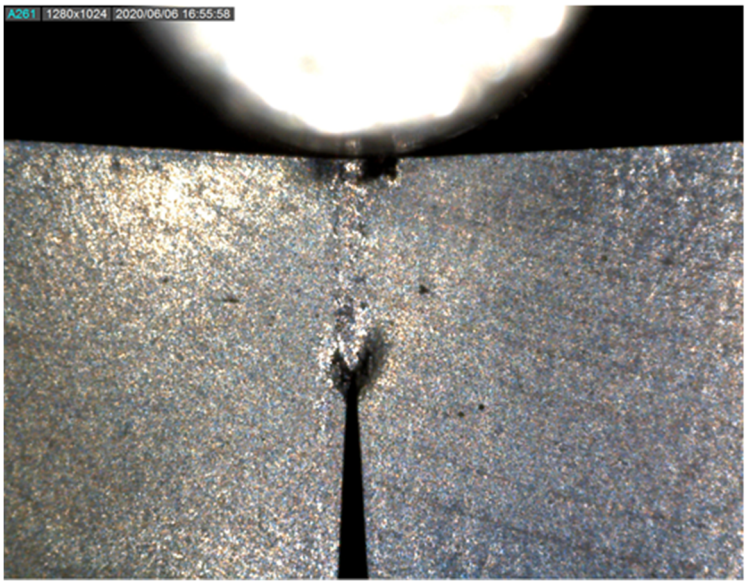

Figure 14. Photo showing the crack-split in the MWCNT-filled SENB sample.

4.5. LSS

4.5.1. Aluminum Bonded Joints

Figure 15 displays the force-displacement curves obtained from the SLS tests conducted on the aluminum bonded specimens. Between the curves, an acceptable deviation is achieved. Figure 16 compares the average values of the LSS of the joints with the MWCNT-filled adhesive with that of joints with the neat adhesive [12]. The comparison shows that the use of the MWCNT-filled adhesive leads to the impressive increase of the LSS by 35.6%, 45% and 57% for the reinforcements of 0.5, 1.0 and 2.0 wt %, respectively. The increase is mainly due to the mechanical interlocking caused by the nano-stitching of the MWCNTs onto the chemically modified surface of the aluminum adherents [20–22] as schematically illustrated in Figure 17.

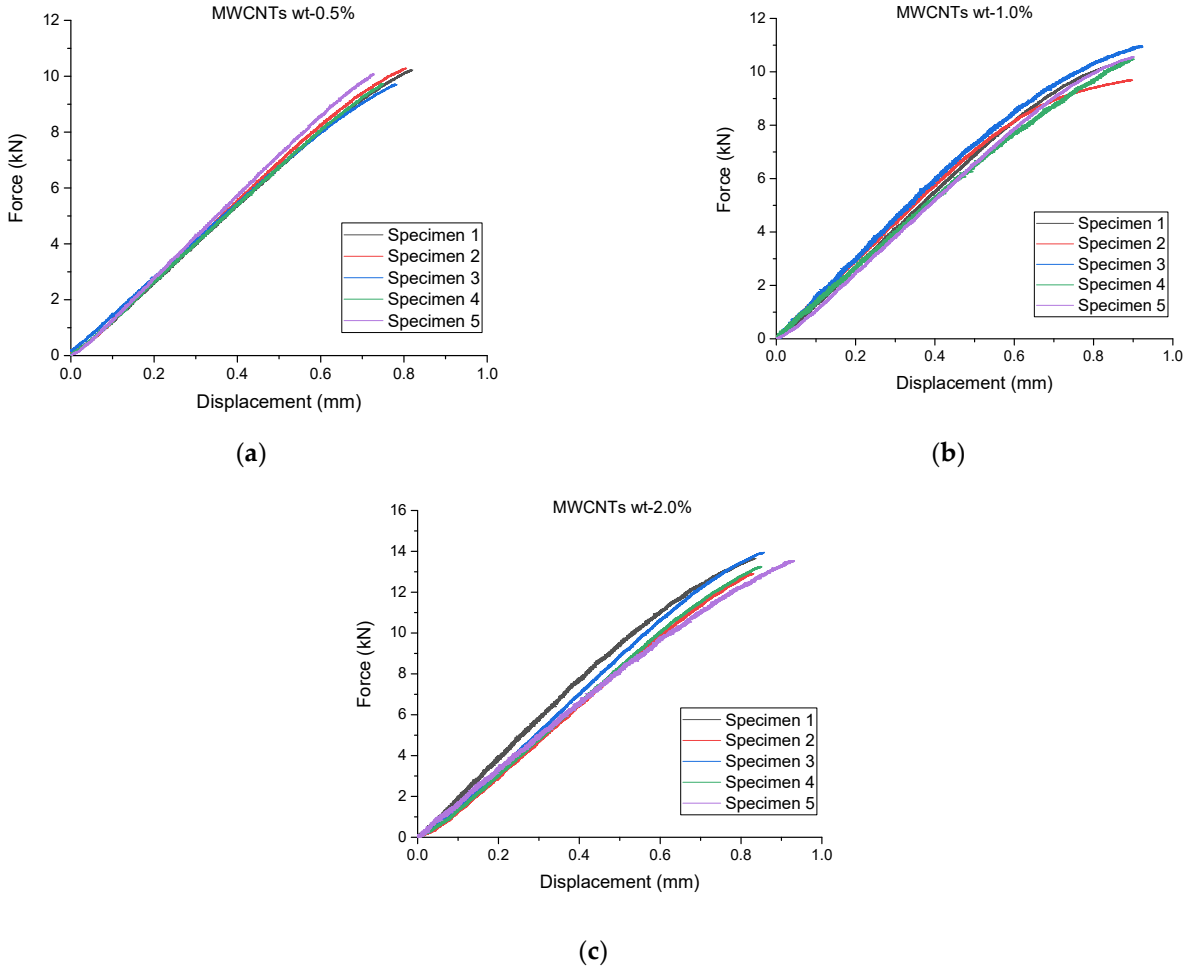

Figure 15. Force-displacement curves of the MWCNT-filled aluminum SLS specimens: (**a**) 0.5 wt %, (**b**) 1.0 wt % and (**c**) 2.0 wt %.

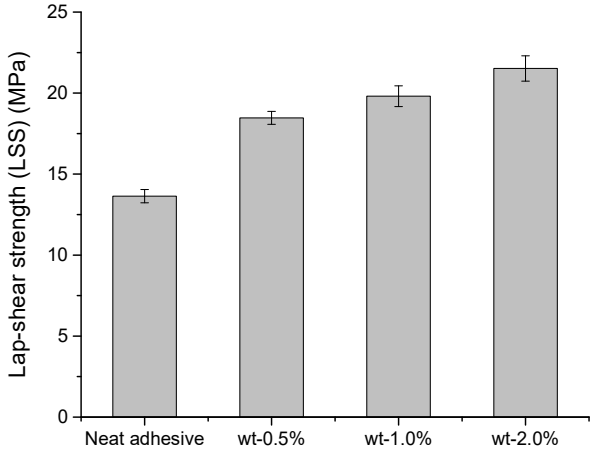

Figure 16. Comparison of the LSS values of the aluminum specimens bonded with the MWCNT-filled adhesive with that of the specimens bonded with the neat adhesive [12].

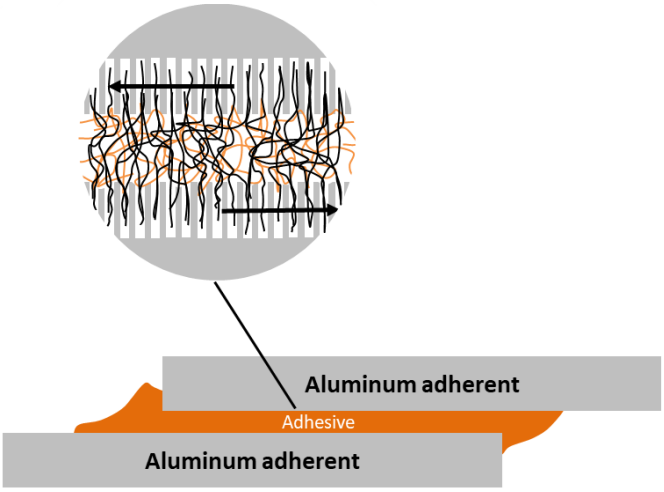

Figure 17. Schematic illustration of the nano-stitching of the MWCNTs onto the chemically modified surface of the aluminum adherent.

In Figure 18, a typical failure surface of the aluminum SLS specimens is shown. The observed failure mode is cohesive, which is an indication of the high quality and high strength of the bonded joints.

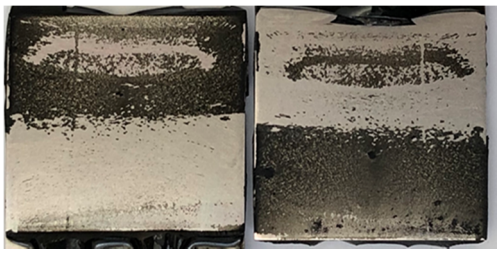

Figure 18. Failure surface of the aluminum specimens bonded with the MWCNT-filled adhesive.

4.5.2. CFRP Bonded Joints

Based on the findings from the SLS tests on the aluminum specimens with the MWCNT-filled adhesive, CFRP specimens were bonded using the MWCNT-filled adhesive of the maximum content (2.0 wt %) and tested. The measured force-displacement curves of the tests are shown in Figure 19. Figure 20 compares the average LSS values of the CFRP specimens bonded with the MWCNT-filled adhesive with that of the specimens bonded with the neat bio-adhesive [12]. The comparison shows an increase of the LSS by 10.4%. The increasing mechanism is the same as in the aluminum bonded specimens (Figure 16). The lower increase of the LSS compared to the one of the aluminum bonded joints is due to the lower activation of the surface of the CFRP adherents applied by the surface treatment (grinding). Nevertheless, the increase of 10% caused by the MWCNTs is significant.

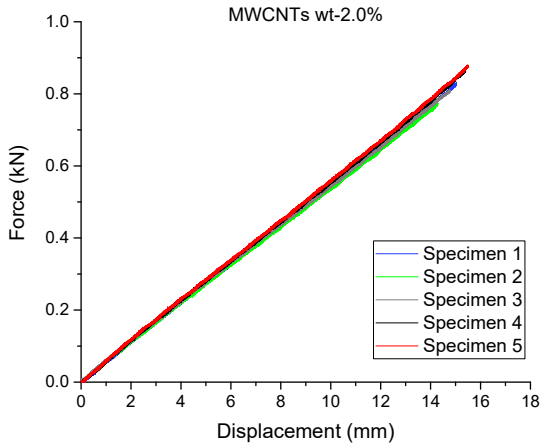

Figure 19. Force-displacement curves of the CFRP SLS specimens bonded with the MWCNT-filled adhesive (2.0 wt %).

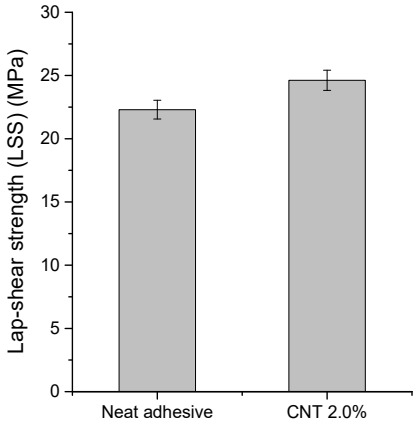

Figure 20. Comparison of the average LSS value of the CFRP specimens bonded with the MWCNT-filled adhesive with that of the CFRP specimens bonded with the neat adhesive [12].

In Figure 21, a typical failure surface of the CFRP SLS specimens is shown. The observed failure mode is cohesive, which is an indication of the high quality and high strength of the bonded joints.

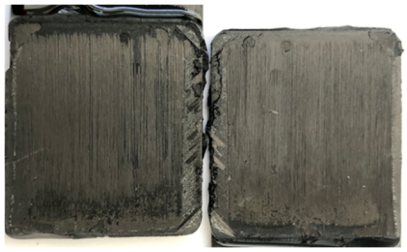

Figure 21. Failure surface of the CFRP SLS specimen bonded with the MWCNT-filled adhesive.

5. Conclusions

In the present work, a novel epichlorohydrin/cardanol adhesive has been reinforced by multi-walled MWCNTs and characterized experimentally as a bulk material and as an adhesive. The results from the tests on bulk samples show that the presence of the MWCNTs increase the adhesive's Young's modulus, the T_g and the fracture toughness of the bio-based adhesive while they decrease the tensile strength. Moreover, the results from

the tests on single lap shear bonded joints show that the presence of MWCNTs increase the lap shear strength of the aluminum joints by 57% and the lap shear strength of the CFRP joints by 10.4%. The findings of the paper, and especially those of the SLS joints, shows that the use of the MWCNTs may lead to a significant increase of the mechanical properties of bio-adhesives.

Author Contributions: Conceptualization, K.T. and V.T.; methodology, K.T. and V.T.; validation, K.T. and V.T.; investigation, V.T.; writing—original draft preparation, K.T.; writing—review and editing, K.T. and V.T.; supervision, K.T.; All authors have read and agreed to the published version of the manuscript.

Funding: This research received no external funding.

Institutional Review Board Statement: Not applicable.

Informed Consent Statement: Informed consent was obtained from all subjects involved in the study.

Data Availability Statement: Not applicable.

Acknowledgments: The authors would like to thank G. Psarras and his team (Department of Materials Science, University of Patras) for their help on the DMA tests and Th. Loutas (Department of Mechanical Engineering & Aeronautics, University of Patras) for providing the CFRP material for the SLS tests.

Conflicts of Interest: The authors declare no conflict of interest.

References

1. Tserpes, K. Adhesive Bonding of Aircraft Structures. In *Revolutionizing Aircraft Materials and Processes*; Pantelakis, S., Tserpes, K., Eds.; Springer: Cham, Switzerland, 2020; pp. 337–357.
2. Pantelakis, S.; Tserpes, K.I. Adhesive bonding of composite aircraft structures: Challenges and recent developments. *Sci. China Phys. Mech. Astron.* **2014**, *57*, 2–11. [CrossRef]
3. Cavezza, F.; Boehm, M.; Terryn, H.; Hauffman, T. A Review on Adhesively Bonded Aluminium Joints in the Automotive Industry. *Metals* **2020**, *10*, 730. [CrossRef]
4. Petrie, E.M. *Handbook of Adhesives and Sealants*; McGraw-Hill Education: New York, NY, USA, 2007.
5. Yi, X.; Tserpes, K. Special Issue "ECO-COMPASS: Ecological and Multifunctional Composites for Application in Aircraft Interior and Secondary Structures". *Aerospace* **2019**, *6*, 17. [CrossRef]
6. Bachmann, J.; Yi, X.; Gong, H.; Martinez, X.; Bugeda, G.; Oller, S.; Tserpes, K.I.; Ramon, E.; Paris, C.; Moreira, P.M.G.P.; et al. Outlook on ecologically improved composites for aviation interior and secondary structures. *CEAS Aeronaut. J.* **2018**, *9*, 533–543. [CrossRef]
7. Luckachan, G.E.; Pillai, C.K. Biodegradable polymers-a review on recent trends and emerging perspectives. *J. Polym. Environ.* **2011**, *9*, 637–676. [CrossRef]
8. Bauer, F.; Decker, U.; Ernst, H.; Findeisen, M.; Langguth, H.; Mehnert, R.; Sauerland, V.; Hinterwaldner, R. Functionalized inorganic/organic nanocomposites as new basic raw materials for adhesives and sealants Part 2. *Int. J. Adhes. Adhes.* **2006**, *26*, 567–570. [CrossRef]
9. Khoee, S.; Hassani, N. Adhesion strength improvement of epoxy resin reinforced with nanoelastomeric copolymer. *Mater. Sci. Eng. A* **2010**, *527*, 6562–6567. [CrossRef]
10. Kinloch, A.J.; Lee, J.H.; Taylor, A.C.; Sprenger, S.; Eger, C.; Egan, D. Toughening structural adhesives via nano-and micro-phase inclusions. *J. Adhes.* **2003**, *79*, 867–873. [CrossRef]
11. Hamid, S.H. *Handbook of Polymer Degradation*; CRC Press: Boca Raton, FL, USA, 2000.
12. Chandra, R.; Rustgi, R. Biodegradable polymers. *Prog. Polym. Sci.* **1998**, *23*, 1273–1335. [CrossRef]
13. Tzatzadakis, V.; Tserpes, K. Production of a novel bio-based structural adhesive and characterization of mechanical properties. *J. Adhes.* **2020**. [CrossRef]
14. Hollaway, L.C. Key issues in the use of fibre reinforced polymer (FRP) composites in the rehabilitation and retrofitting of concrete structures. In *Service Life Estimation and Extension of Civil Engineering Structures*; Woodhead Publishing: Cambridge, UK, 2011; pp. 3–74.
15. Rodrigues, F.H.; Franca, F.C.; Souza, J.R.; Ricardo, N.M.; Feitosa, J. Comparison between physico-chemical properties of the technical Cashew Nut Shell Liquid (CNSL) and those natural extracted from solvent and pressing. *Polimeros* **2011**, *21*, 156–160. [CrossRef]
16. ASTM D5045-14. *Standard Test Methods for Plane-Strain Fracture Toughness and Strain Energy Release Rate of Plastic Materials*; ASTM International: West Conshohocken, PA, USA, 2014.

17. Tzatzadakis, V.; Tserpes, K. Experimental characterization of the hygrothermal ageing effects on the bulk mechanical properties and lap-shear strength of the novel bio-based epichlorohydrin/cardanol adhesive. *J. Adhes.* **2020**. [CrossRef]
18. Mach, P.; Geczy, A.; Polansky, R.; Busek, D. Glass transition temperature of nanoparticle-enhanced and environmentally stressed conductive adhesive materials for electronics assembly. *J. Mater. Sci. Mater. Electron.* **2019**, *30*, 4895–4907. [CrossRef]
19. Tserpes, K.I.; Moutsompegka, E.; Murariu, O.; Bonnaud, L.; Chanteli, A. Experimental investigation of the effect of hygrothermal aging on the mechanical performance of carbon nanotube/PA6 nanocomposite. *Plast. Rubber Compos.* **2017**, *46*, 239–244. [CrossRef]
20. Chanteli, A.; Tserpes, K.I. Tensile behaviour of carbon nanotube/polypropylene composite material. *Plast. Rubber Compos.* **2014**, *43*, 330–336. [CrossRef]
21. Gkikas, G.; Sioulas, D.; Lekatou, A.; Barkoula, N.M.; Paipetis, A.S. Enhanced bonded aircraft repair using nano-modified adhesives. *Mater. Des.* **2012**, *41*, 394–402. [CrossRef]
22. Barra, G.; Vertuccio, L.; Vietri, U.; Naddeo, C.; Hadavinia, H.; Guadagno, L. Toughening of epoxy adhesives by combined interaction of carbon nanotubes and silsesquioxanes. *Materials* **2017**, *10*, 1131. [CrossRef] [PubMed]